

## Supporting Information

### **Interlayer engineering in V<sub>6</sub>O<sub>13</sub> nanobelts toward superior Mg-ion storage**

Huabin Kong<sup>†\*a</sup>, Jianxin Ou<sup>†a</sup>, Lu Chen<sup>a</sup>, Wenlu Sun<sup>a</sup>, Fang Fu<sup>a</sup>, Hui Zhang<sup>\*b</sup>,  
Hongwei Chen<sup>\*a</sup>

<sup>a</sup>Department of Materials Science and Engineering, Huaqiao University, Xiamen,  
361021, China

<sup>b</sup>National Key Laboratory of High-efficiency Utilization of Coal and Green Chemical  
Engineering, Ningxia University, Yinchun, 750021, China

#These authors contributed equally to this work

Corresponding authors.

\*Huabin Kong, E-mail: konghuabin@hqu.edu.cn

\*Hui Zhang, E-mail: zhang\_hui0058@nxu.edu.cn

\*Hongwei Chen, E-mail: hwchen@hqu.edu.cn

## **Material Characterizations**

The composition and purity of the material were characterized by X-ray diffraction (XRD) on Bruker D8-advance X-ray diffractometer with Cu-K $\alpha$  radiation ( $\lambda=1.5418$  Å), using an operating voltage and current of 40 kV and 40 mA. FTIR spectrums were collected using a ThermoScientific Nicolet 6700 spectrometer. Raman spectra were recorded using a Jobin Yvon LabRam HR 800 confocal micro-Raman system. SEM images were obtained with a FEI Quanta 400 FEG equipped with EDX (Apollo 40 SDD) operated at 10 kV. TEM images were recorded using a Tecnai G2 F20 S-TWIN at 200 kV. XPS spectra were collected using Thermo Scientific ESCALAB 250Xi with Al Ka radiation. The pressure in the analysis chamber was typically  $2 \times 10^{-9}$  torr during acquisition. All reported binding energy values are calibrated to the graphitic C1s peak with a value of 284.6 eV. Combined DTA-TG measurement was conducted in a SETARAM DSC-141 at a heating rate of  $10 \text{ K min}^{-1}$  in air atmosphere.

## **Electrochemical Measurements**

The electrochemical evaluation was performed on 2032-type coin cells. The prepared electrode material, carbon black and poly(vinyl difluoride) (PVDF) were mixed in a weight ratio of 7:2:1. Slurry of the mixture was stirred for 12 h and pasted on copper foil, followed by the electrode film being dried in vacuum at  $100 \text{ }^\circ\text{C}$  for 12 h. The average mass loading of active materials was  $\sim 1.5 \text{ mg cm}^{-2}$ . For MIBs cell, activated carbon was used as the anode and the  $0.5 \text{ M Mg(TFSI)}_2$  in ethylene glycol dimethyl ether (DME) as the electrolyte. Cell assembly was performed in glovebox. The cyclic

voltammetry (CV) and electrochemical impedance spectroscopy (EIS) measurements were performed on CHI604C electrochemical workstation with a voltage range from 0.4 to -1.6 V at a scanning rate of 0.5 mV s<sup>-1</sup>. The galvanostatic charge/discharge measurements were performed on a battery testing system (NEWARE, NEWARE technology Ltd. Shenzhen) with a voltage of -1.6–0.4 V. For the GITT tests, the cell was discharged/charged at 0.1 A g<sup>-1</sup> with current pulse duration of 5 min and interval time of 20 min.

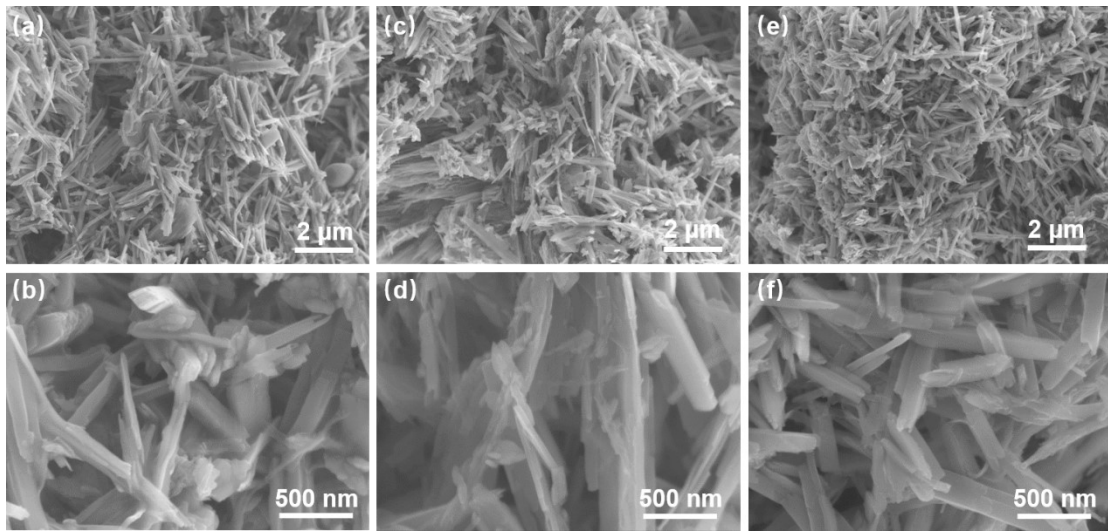


**Fig. S1** The SEM images of (a, b) V<sub>6</sub>O<sub>13</sub>, (c, d) PA50-V<sub>6</sub>O<sub>13</sub> and (e, f) PA150-V<sub>6</sub>O<sub>13</sub>.

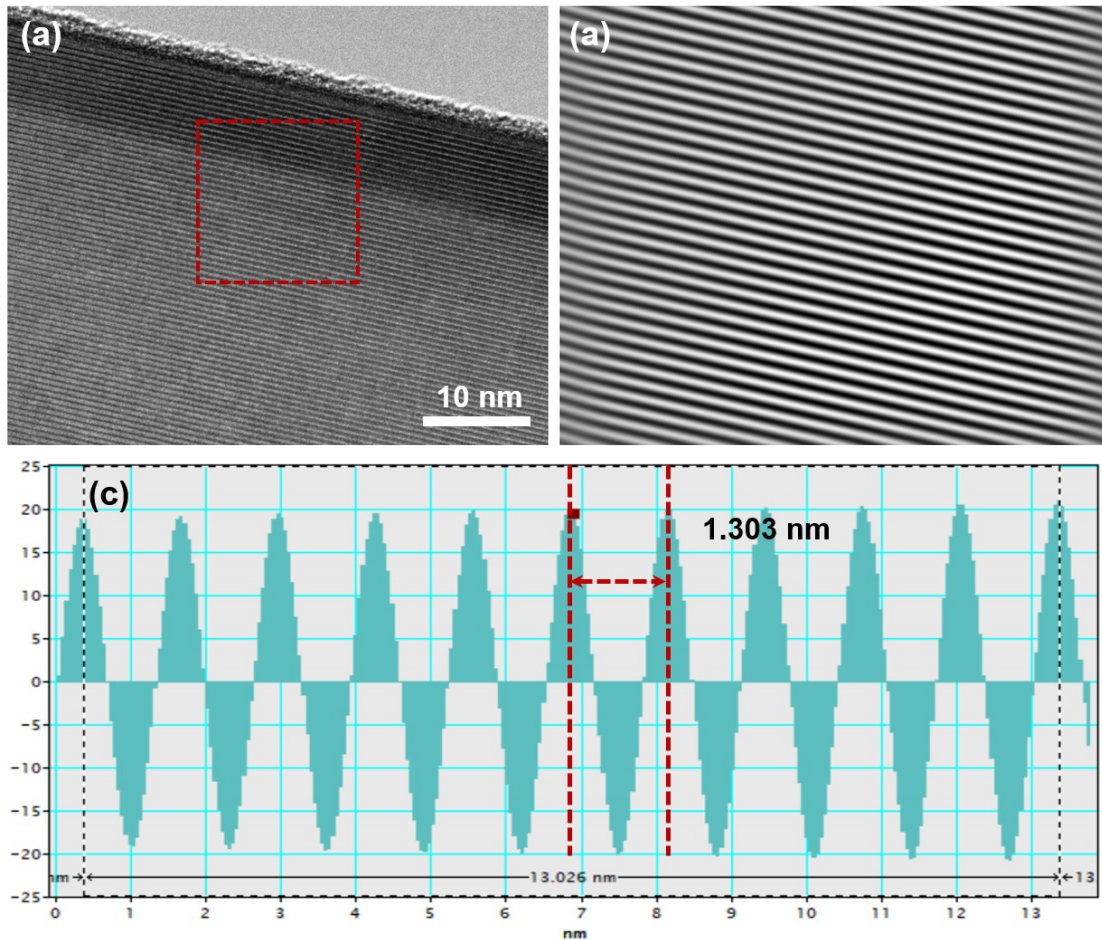


**Fig. S2** Microstructure analysis of the PA100- $V_6O_{13}$ . (a) HRTEM images, (b) Inverse-FFT images of selected regions, (c) Corresponding intensity line-profile indicating the interlayer spacing.

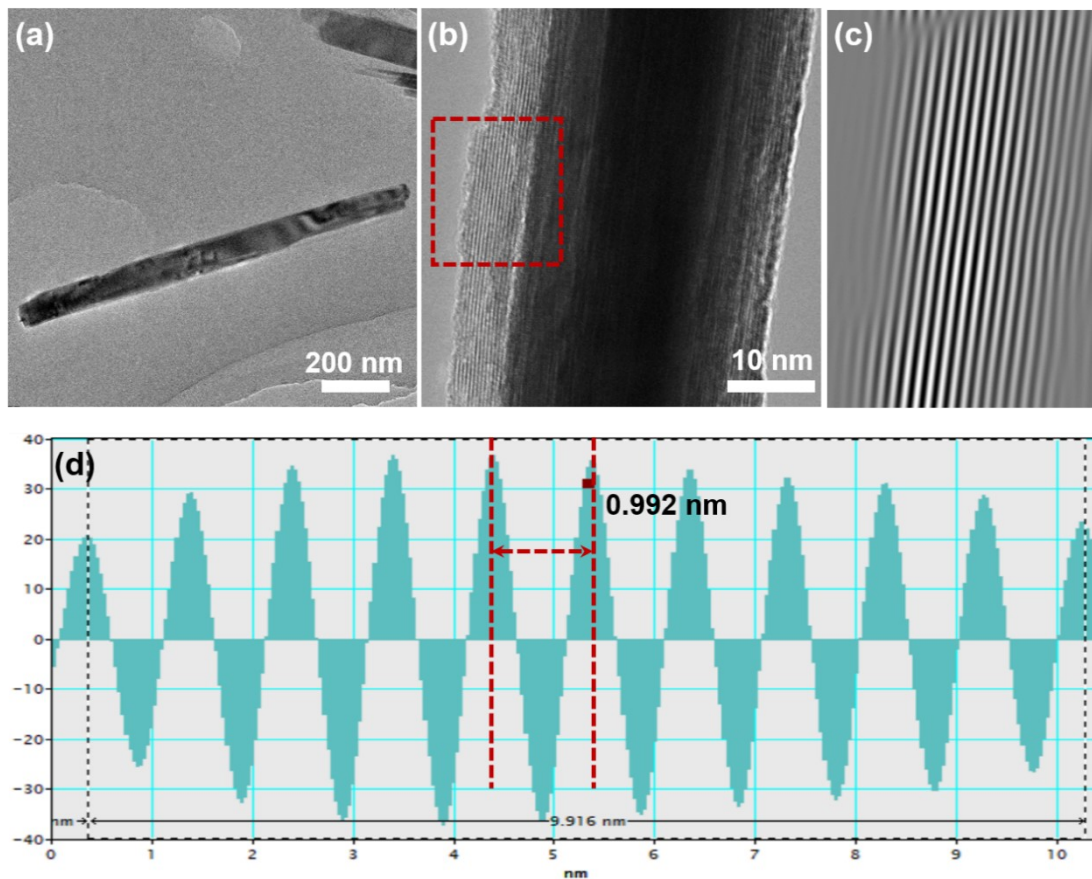


**Fig. S3** Microstructure analysis of the  $V_6O_{13}$ . (a) TEM image, (b) HRTEM images, (c) Inverse-FFT images of selected regions, (d) Corresponding intensity line-profile indicating the interlayer spacing.

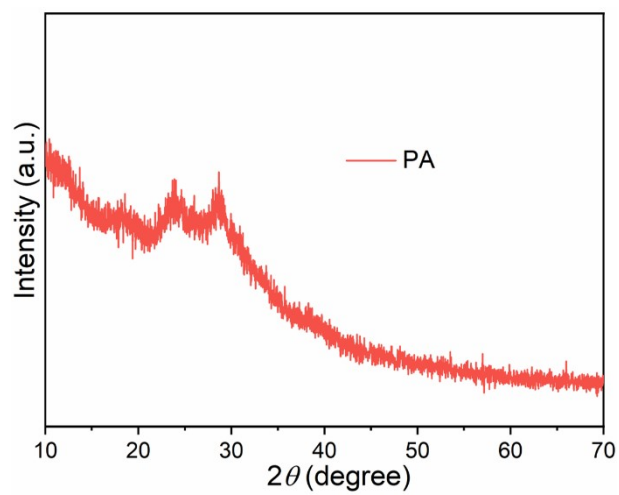


**Fig. S4.** XRD pattern of PA.

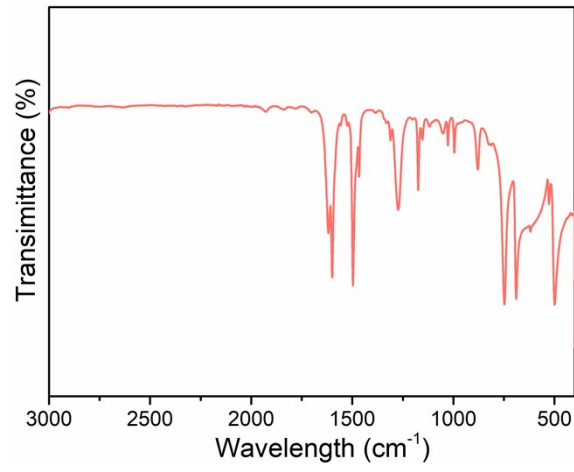


**Fig. S5** FTIR spectrum of aniline monomer.



**Table S1.** Elemental analysis results of PA100-V<sub>6</sub>O<sub>13</sub>.

Element	C	N	H
Weight%	7.43	1.45	0.38

**Calculation process of each substance content in the PA100-V<sub>6</sub>O<sub>13</sub>**

After the TG measurement, the final remaining product is V<sub>2</sub>O<sub>5</sub>. According to the proportion of V<sub>2</sub>O<sub>5</sub> (93.68%), it can be calculated that the percentage of V<sub>6</sub>O<sub>13</sub> in the PA100-V<sub>6</sub>O<sub>13</sub> is 88.18%. Subsequently, based on the results of elemental analysis measurement, the amount of PA can be calculated to be 9.60%.

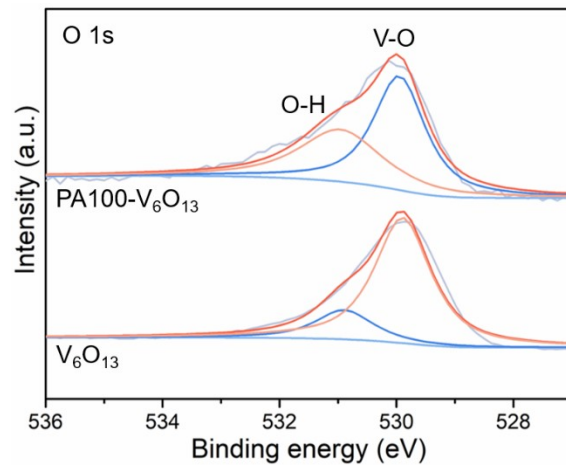


**Fig. S6** O 1s XPS spectra of V<sub>6</sub>O<sub>13</sub> and PA100-V<sub>6</sub>O<sub>13</sub>.

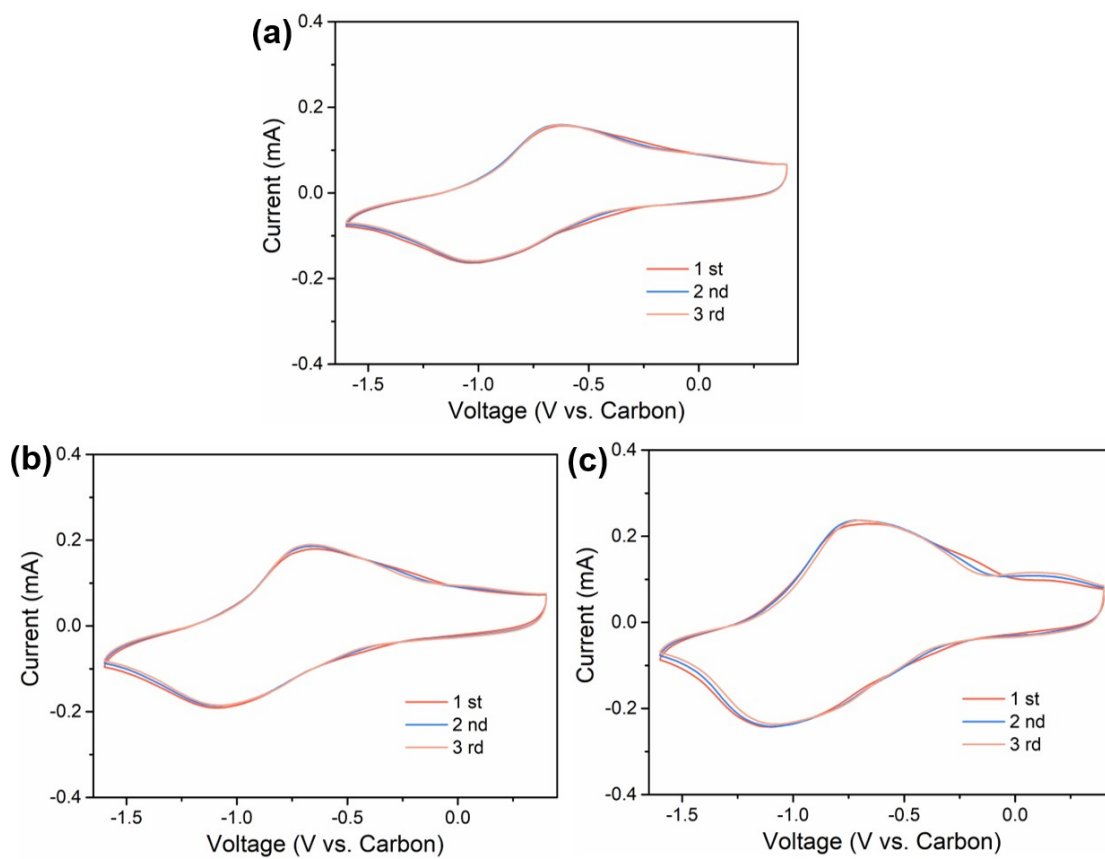


**Fig. S7** The CV curves of samples at a scan rate of  $0.5 \text{ mV s}^{-1}$ : (a)  $\text{V}_6\text{O}_{13}$ , (b) PA50- $\text{V}_6\text{O}_{13}$ , (c) PA150- $\text{V}_6\text{O}_{13}$ .

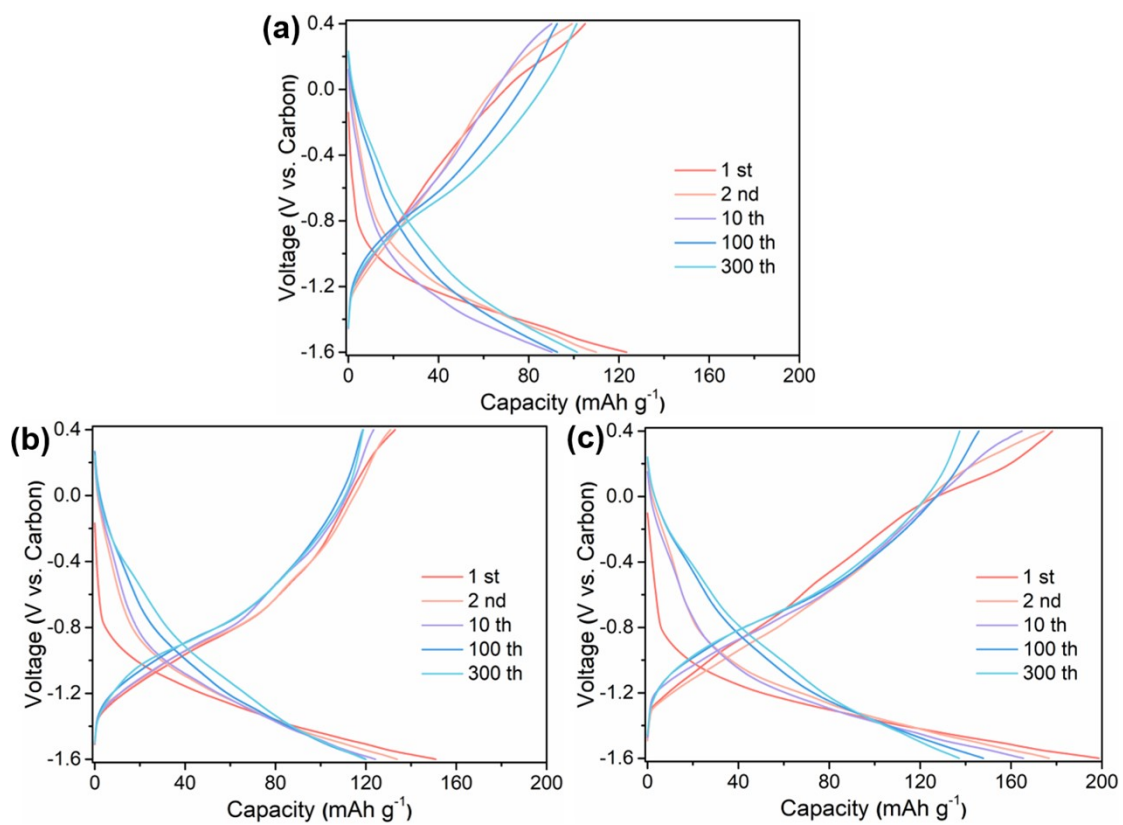


**Fig. S8** The charge/discharge profiles of samples at a current density of  $0.1 \text{ A g}^{-1}$ : (a)

$\text{V}_6\text{O}_{13}$ ,

(b)

$\text{PA50-V}_6\text{O}_{13}$ ,

(c)

$\text{PA150-V}_6\text{O}_{13}$ .

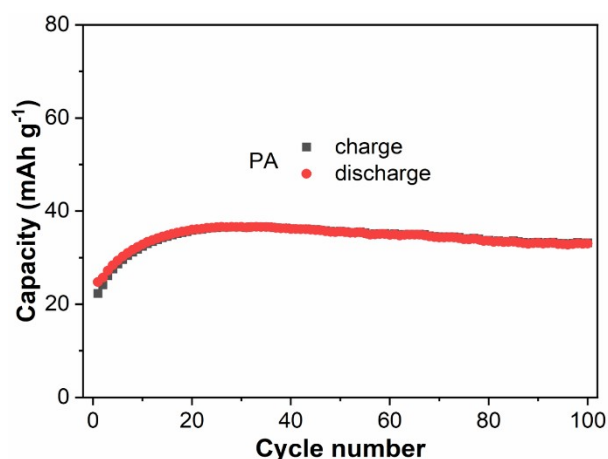


**Fig S9** Cycling performance of PA at  $0.1 \text{ A g}^{-1}$ .

**Theoretical capacity calculation:**

As shown in Fig 4c and Fig S9, the discharge capacity of PA100- $\text{V}_6\text{O}_{13}$  and PA are 173 and 100  $\text{mAh g}^{-1}$  at the 100 th cycle. According to the results of TG and elemental analysis (Fig. 3c and Table S1), it can be known that the contents of  $\text{V}_6\text{O}_{13}$ , PA and adsorbed water in the PA100- $\text{V}_6\text{O}_{13}$  are 88.18%, 9.60% and 2.22%, respectively. Therefore, it can be calculated that the PA provides a capacity of  $3.2 \text{ mAh g}^{-1}$  ( $33 \text{ mAh g}^{-1} \times 9.6\% = 3.2 \text{ mAh g}^{-1}$ ) and the  $\text{V}_6\text{O}_{13}$  provides a capacity of  $169.8 \text{ mAh g}^{-1}$  ( $173 \text{ mAh g}^{-1} - 3.2 \text{ mAh g}^{-1} = 169.8 \text{ mAh g}^{-1}$ ). Therefore, the capacity contributed by the  $\text{V}_6\text{O}_{13}$  and PA account for 1.85% ( $(3.2 \text{ mAh g}^{-1} / 173 \text{ mAh g}^{-1}) \times 100\% = 1.85\%$ ) and 98.15% ( $(169.8 \text{ mAh g}^{-1} / 173 \text{ mAh g}^{-1}) \times 100\% = 98.15\%$ ) of the total capacity, respectively.

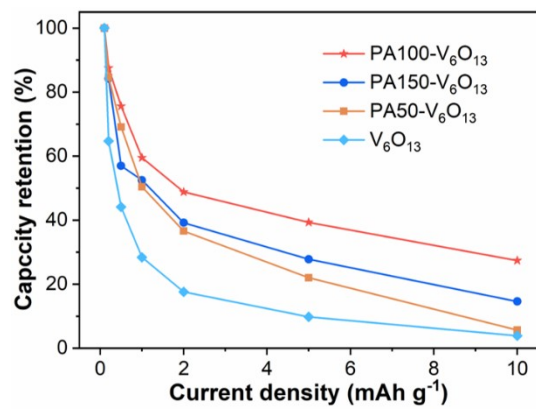


**Fig. S10** Capacity retention curves of four electrodes at different current densities.

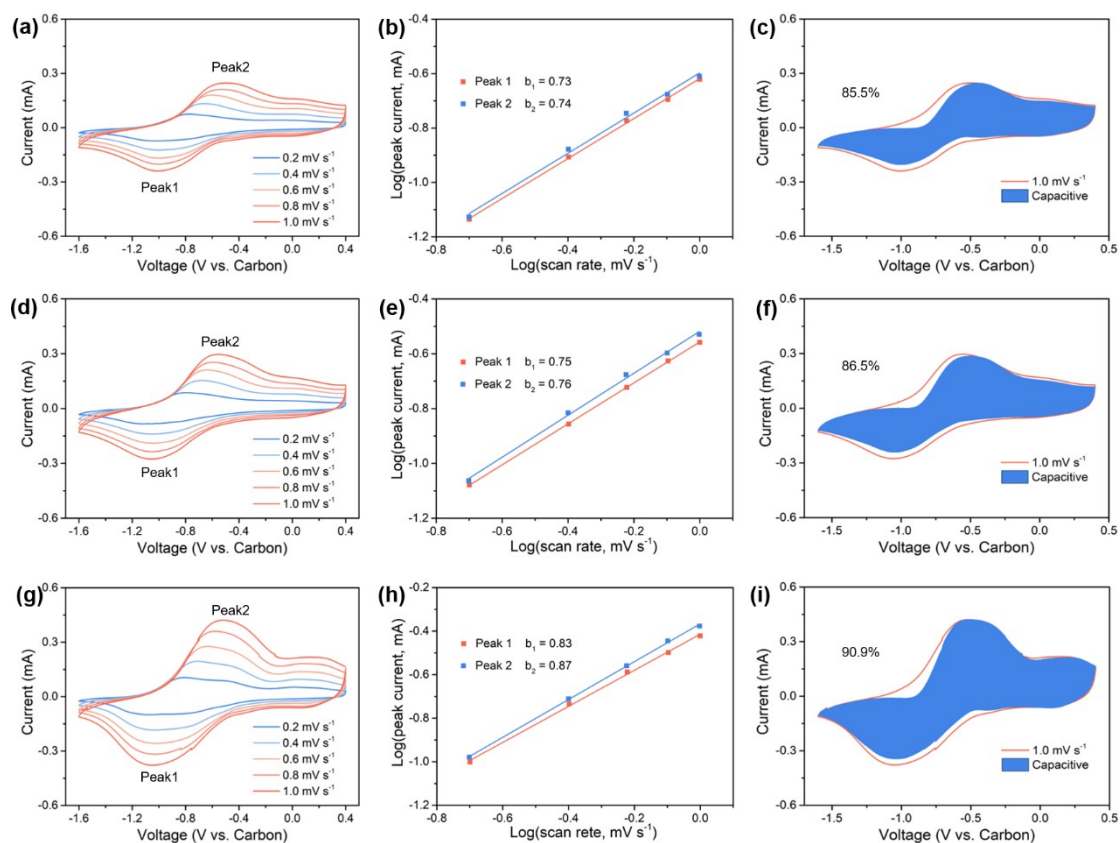


**Fig. S11** Kinetics analysis of the electrochemical behavior towards  $\text{Mg}^{2+}$  for the  $\text{V}_6\text{O}_{13}$ ,  $\text{PA50-V}_6\text{O}_{13}$  and  $\text{PA150-V}_6\text{O}_{13}$ : (a, d, g) CV curves at various scan rates from 0.2 to 1.0  $\text{mV s}^{-1}$ , (b, e, h) the determination of the  $b$ -value using the relationship between the peak current and scan rate, (c, f, i) the separation of the capacitive and diffusion currents at a scan rate of 1.0  $\text{mV s}^{-1}$ , the capacitive contribution to the total current is shown *via* the shaded region.

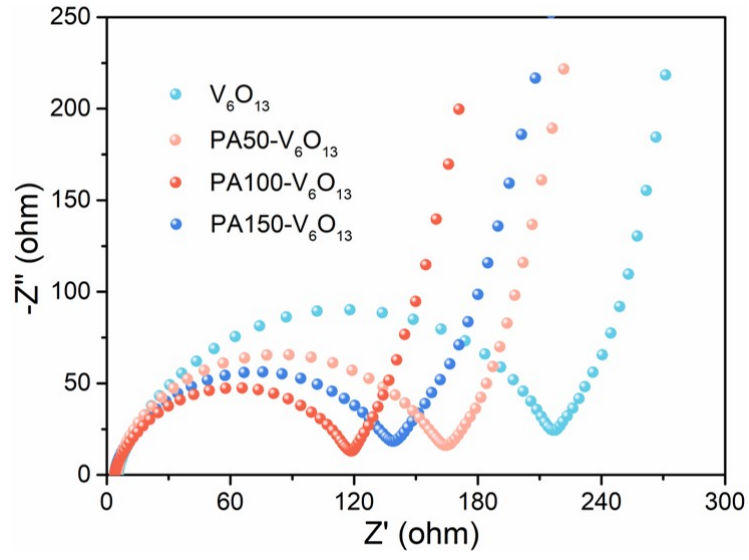


**Fig. S12** The Nyquist plots of samples before cycling.



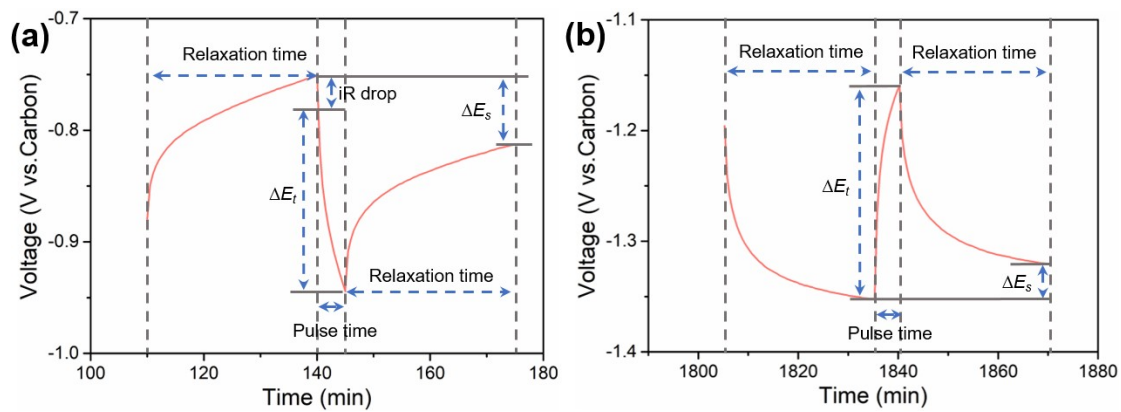


**Fig. S13** E vs. t curves of the PA100-V<sub>6</sub>O<sub>13</sub> for a single GITT during discharge/charge process.

The lithium diffusion coefficient was measured by using Galvanostatic intermittent titration technique (GITT) and calculated based on equation as follows.<sup>[1, 2]</sup>

$$D = \frac{4L^2}{\pi\tau} \left( \frac{\Delta E_s}{\Delta E_t} \right)^2$$

Where  $L$  is lithium ion diffusion length (unit: cm); for compact electrode, it is equal to average thickness of pole piece measured,  $\tau$  is the relaxation time (unit: s), and  $\Delta E_s$  is the steady-state potential (unit: V) by the current pulse.  $\Delta E_t$  is the potential change (unit: V) during the constant current pulse after eliminating the  $iR$  drop.

[1] G. Fang, G. Fang, Q. Wang, J. Zhou, Y. Lei, Z. Chen, Z. Wang, A. Pan, S. Liang, Metal organic framework-templated synthesis of bimetallic selenides with rich phase boundaries for sodium-ion storage and oxygen evolution reaction, *ACS Nano*, 2019, 13, 5635-5645.

[2] D. T. Ngo, H. T. Le, C. Kim, J-Y Lee, J. G. Fisher, I-D. Kim, C-J. Park, Mass-scalable synthesis of 3D porous germanium-carbon composite particles as an ultra-high rate anode for lithium ion batteries, *Energy Environ. Sci.*, 2015, 8, 3577-3588.